

Maxwellian gas undergoing a stationary Poiseuille flow in a pipe

Mohamed Sabbane, Mohamed Tij

Département de Physique, Université Moulay Ismaïl, Meknès, Morocco

Andrés Santos*

Departamento de Física, Universidad de Extremadura, E-06071 Badajoz, Spain

Abstract

The hierarchy of moment equations derived from the nonlinear Boltzmann equation is solved for a gas of Maxwell molecules undergoing a stationary Poiseuille flow induced by an external force in a pipe. The solution is obtained as a perturbation expansion in powers of the force (through third order). A critical comparison is done between the Navier–Stokes theory and the predictions obtained from the Boltzmann equation for the profiles of the hydrodynamic quantities and their fluxes. The Navier–Stokes description fails to first order and, especially, to second order in the force. Thus, the hydrostatic pressure is not uniform, the temperature profile exhibits a non-monotonic behavior, a longitudinal component of the flux exists in the absence of longitudinal thermal gradient, and normal stress differences are present. On the other hand, comparison with the Bhatnagar–Gross–Krook model kinetic equation shows that the latter is able to capture the correct functional dependence of the fields, although the numerical values of the coefficients are in general between 0.38 and 1.38 times the Boltzmann values. A short comparison with the results corresponding to the planar Poiseuille flow is also carried out.

Key words: Poiseuille flow, Non-Newtonian properties, Kinetic theory, Boltzmann equation, Maxwell molecules

PACS: 05.20.Dd, 05.60.-k, 47.50.+d

* Corresponding author

Email addresses: mtij@fsmek.ac.ma (Mohamed Tij), andres@unex.es (Andrés Santos).

URL: <http://www.unex.es/fisteor/andres> (Andrés Santos).

1 Introduction

The Poiseuille flow, first studied by Hagen and Poiseuille towards the half of the 19th century, is still one of the classical examples in fluid dynamics [1]. It describes the steady flow in a slab or in a pipe under the action of a longitudinal pressure gradient, what produces a longitudinal macroscopic velocity with a typical parabolic profile in the transverse directions. Essentially the same effect is generated when the longitudinal pressure difference is replaced by a uniform external force $m\mathbf{g}$ (e.g. gravity) directed longitudinally. This latter mechanism for driving the Poiseuille flow does not produce longitudinal gradients and so is more convenient than the former in computer simulations as well as from the theoretical point of view, especially to assess the reliability of the continuum description [2,3,4,5,6,7,8,9,10,11,12,13,14,15,16]. The first study of the Poiseuille flow driven by an external force we are aware of was carried out by Kadanoff *et al.* [2], who simulated the flow with the FHP lattice gas automaton [17] to confirm the validity of a hydrodynamic description for lattice gas automata. In the context of a dilute gas, Esposito *et al.* [3] studied the Boltzmann equation and found that if the force is sufficiently weak there is a solution which converges, in the hydrodynamic limit, to the local equilibrium distribution with parameters given by the stationary solution of the Navier–Stokes (NS) equations. A generalized Navier–Stokes theory was seen to give a reasonable account of a fluid composed of molecules with spin when compared with molecular dynamics simulations [4].

The first kinetic theory analysis of the Poiseuille flow clearly exhibiting non-Newtonian behavior was carried out by Alaoui and Santos [5], who found an exact solution of the Bhatnagar–Gross–Krook (BGK) model kinetic equation for a particular value of g . The general solution of the BGK model under the form of an expansion in powers of g through fifth order was obtained by Tij and Santos [6]. The most interesting outcome of the solution, as first recognized by Malek Mansour *et al.* [7], was the presence of a positive quadratic term in the temperature profile to second order in g , in addition to the negative quartic term predicted by the NS description. As a consequence of this new term, the temperature profile exhibits a bimodal shape, namely a local minimum at the middle of the channel surrounded by two symmetric maxima at a distance of a few mean free paths. In contrast, the continuum hydrodynamic equations predict a temperature profile with a (flat) maximum at the middle. The Fourier law is dramatically violated since in the slab enclosed by the two maxima the transverse component of the heat flux is parallel (rather than anti-parallel) to the thermal gradient. This phenomenon is not an artifact of the BGK model since the same results, except for the numerical values of the coefficients, were derived from an exact solution of the Boltzmann equation for Maxwell molecules through second order [8], as well as from approximate solutions of the Boltzmann equation for hard spheres by Grad’s moment method [9,10]. It

is interesting to note that this correction to the NS temperature profile is not captured by the next hydrodynamic description, namely the Burnett equations [11]. Therefore, in order to describe a non-monotonic temperature field [which is an $\mathcal{O}(g^2)$ -order effect] from a hydrodynamic description one needs to go at least to the super-Burnett equations [8]. A systematic asymptotic analysis of the BGK equation with diffuse boundary conditions to second order in the Knudsen number [12] validates the results of Ref. [6] as corresponding to the Taylor series expansion of the normal (or Hilbert) solution around the center of the gap. The theoretical predictions of a bimodal temperature profile have been confirmed at a qualitative and semi-quantitative level by numerical Monte Carlo simulations of the Boltzmann equation [7,11] and by molecular dynamics simulations [9,13]. In the case of a *dense* gas, even though the non-monotonic behavior of the temperature profile may disappear, the existence of a quadratic term coexisting with the classical quartic term is supported by molecular dynamics simulations [14]. It is worth mentioning that when the Poiseuille flow is driven by a longitudinal pressure gradient rather than by an external force, the NS description is in much better agreement with Monte Carlo simulations of the Boltzmann equation [15].

Practically all the studies about the Poiseuille flow driven by an external force have considered the *planar* geometry [2,3,4,5,6,7,8,9,10,11,12,13,14,15], i.e. the fluid is assumed to be enclosed between two parallel, infinite plates orthogonal to the y -direction, the force acting along the z -direction. In the stationary laminar flow the physical quantities have a unidirectional dependence on the y coordinate only. While the planar geometry is the simplest one to study the Poiseuille flow, it is much more realistic to consider that the fluid is enclosed in a cylindrical pipe, the external force being directed along the symmetry axis z . In that case, the quantities depend on the distance $r = \sqrt{x^2 + y^2}$ from the axis and the fluxes have in general both radial and tangential components. Two of us have recently solved the BGK model for the cylindrical Poiseuille flow through fourth order in g [16]. The results showed that the structure of the hydrodynamic and flux profiles in the pipe geometry is similar to that of the slab geometry. In particular, the temperature exhibits a non-monotonic behavior as one moves apart from the pipe axis. On the other hand, the results are quantitatively sensitive to the geometry of the problem. For instance, the normal stress along the gradient direction is uniform in the planar case ($P_{yy} = \text{const}$), while it has a non-trivial spatial dependence in the cylindrical case ($P_{rr} \neq \text{const}$). Also, comparison with the BGK solution for the planar geometry [6] shows that the differences between the kinetic theory results and the NS predictions are in general more pronounced in the planar case than in the cylindrical case.

As is well known, in the BGK model kinetic equation the complicated non-linear structure of the Boltzmann collision operator is replaced by a single relaxation-time term to the local equilibrium distribution [18]. This is usually

sufficient to account for many of the nonequilibrium properties of the underlying Boltzmann equation, at least at a qualitative level [19]. However, the existence of only one effective collision frequency does not allow the BGK model to describe quantitatively those states where momentum and heat fluxes coexist and are inextricably intertwined, as happens in the Poiseuille flow. This limitation of the BGK model is responsible for an incorrect value $\text{Pr} = 1$ of the Prandtl number [18], in contrast to the Boltzmann value [18,20] $\text{Pr} \simeq \frac{2}{3}$. In the planar Poiseuille flow, it is possible to assess the validity of the BGK solution [6] by comparing it with the results derived from the Boltzmann equation for Maxwell molecules [8] and hard spheres [9,10]. The aim of this paper is to fill the gap caused by the absence of results from the Boltzmann equation for the cylindrical Poiseuille flow. We consider a gas of Maxwell molecules and solve the infinite hierarchy of moment equations stemming from the Boltzmann equation through third order in the external force. The results confirm the correctness of the functional dependence of the hydrodynamic and flux profiles obtained from the BGK model [16]. On the other hand, the numerical values of the coefficients are in general different in both kinetic theories, as expected. The organization of the paper is the following. Section 2 is devoted to the description of the flow under study and its solution in a hydrodynamic description to NS order. The kinetic theory description is presented in Sec. 3. In order to solve the moment hierarchy in a systematic and recursive way, we carry out a perturbation expansion in powers of the external field in Sec. 4, the technical details being relegated to Appendix B. The results are extensively discussed and compared with those of the NS and BGK descriptions in Sec. 5. Finally, the main conclusions of the paper are briefly presented in Sec. 6.

2 Navier–Stokes description of the cylindrical Poiseuille flow

The cylindrical Poiseuille flow studied in this paper refers to a monatomic dilute gas enclosed in a long pipe of radius R . Let us take the z -axis as the symmetry axis of the cylinder. The gas particles are subjected to the action of a constant external force per unit mass $\mathbf{g} = g\hat{\mathbf{z}}$ (e.g. gravity) parallel to z . After a certain transient stage, the system reaches a steady laminar flow. This nonequilibrium state is characterized by gradients of the hydrodynamic variables along the directions x and y orthogonal to the cylinder axis. By symmetry, the hydrodynamic fields are expected to depend on x and y through the distance $r = \sqrt{x^2 + y^2}$ from the z -axis. In our analysis, we are interested in the bulk region of the flow. This means that the radius R of the cylinder is assumed to be large enough (as compared with the mean free path) to allow for the existence of such a region.

The *steady-state* balance equations expressing the conservation of momentum

and energy are

$$\nabla \cdot \mathbf{P} = \rho \mathbf{g}, \quad (1)$$

$$\nabla \cdot \mathbf{q} + \mathbf{P} : \nabla \mathbf{u} = 0, \quad (2)$$

where ρ is the mass density, $\mathbf{u} = u_z \hat{\mathbf{z}}$ is the flow velocity, \mathbf{P} is the pressure tensor and \mathbf{q} is the heat flux vector. The geometry of the problem suggests the use of cylindrical coordinates (see Appendix A). Using Eqs. (A.8)–(A.12), Eqs. (1) and (2) yield

$$\frac{\partial}{\partial r} (r P_{rr}) = P_{\phi\phi}, \quad (3)$$

$$\frac{1}{r} \frac{\partial}{\partial r} (r P_{rz}) = \rho g, \quad (4)$$

$$P_{rz} r \frac{\partial u_z}{\partial r} + \frac{\partial}{\partial r} (r q_r) = 0, \quad (5)$$

Equations (3)–(5) are exact, but they do not constitute a closed set.

In the Navier–Stokes (NS) description, the momentum and heat fluxes are assumed to be linear functions of the hydrodynamic gradients [1,18,20]. In the geometry of the cylindrical Poiseuille flow the NS constitutive equations are written as

$$P_{rr} = P_{\phi\phi} = P_{zz} = p, \quad (6)$$

$$P_{rz} = -\eta \frac{\partial u_z}{\partial r}, \quad (7)$$

$$q_r = -\kappa \frac{\partial T}{\partial r}, \quad (8)$$

$$q_z = 0. \quad (9)$$

In Eq. (6), $p = \frac{1}{3} \text{tr} \mathbf{P}$ is the hydrostatic pressure. Equation (7) is Newton’s friction law, η being the shear viscosity. In addition, Eq. (8) is Fourier’s law, where κ is the thermal conductivity and T is the temperature. The latter is related to the number density $n = \rho/m$ (where m is the mass of a particle) and the pressure p by the (local) equilibrium equation of state. In particular, for a dilute gas, $p = nk_B T$, k_B being the Boltzmann constant. Equation (6) implies the absence of normal stress differences in a sheared Newtonian fluid, while Eq. (9) means that the heat flux is parallel to the thermal gradient in a fluid obeying Fourier’s law. The combination of Eqs. (3)–(8) gives the following closed set of hydrodynamic equations:

$$\frac{\partial p}{\partial r} = 0, \quad (10)$$

$$r^{-1} \frac{\partial}{\partial r} \left(r \eta \frac{\partial u_z}{\partial r} \right) = -\rho g, \quad (11)$$

$$\frac{\partial}{\partial r} \left(r \kappa \frac{\partial T}{\partial r} \right) = -\eta r \left(\frac{\partial u_z}{\partial r} \right)^2. \quad (12)$$

In principle, the NS hydrodynamic equations (10)–(12) are too complicated to obtain its explicit solution for arbitrary g . On the other hand, the solution can be found as a series expansion in powers of g . To third order the result is

$$p(r) = p_0, \quad (13)$$

$$u_z(r) = u_0 - \frac{\rho_0 g}{4\eta_0} r^2 \left(1 + \frac{1}{144} \frac{\rho_0^2 g^2}{\eta_0 \kappa_0 T_0} r^4 \right) + \mathcal{O}(g^5), \quad (14)$$

$$T(r) = T_0 - \frac{1}{64} \frac{\rho_0^2 g^2}{\eta_0 \kappa_0} r^4 + \mathcal{O}(g^4), \quad (15)$$

where we have particularized to a dilute gas of Maxwell molecules, in which case $\eta \propto T$ and $\kappa \propto T$ [18,20]. The subscript 0 in Eqs. (13)–(15) denotes quantities evaluated at $r = 0$, i.e. $u_0 = u_z(0)$, $T_0 = T(0)$, $\eta_0 = \eta(T_0)$, \dots . The corresponding expressions for the fluxes are

$$P_{rz}(r) = \frac{\rho_0 g}{2} r \left(1 + \frac{1}{192} \frac{\rho_0^2 g^2}{\eta_0 \kappa_0 T_0} r^4 \right) + \mathcal{O}(g^5), \quad (16)$$

$$q_r(r) = \frac{1}{16} \frac{\rho_0^2 g^2}{\eta_0} r^3 + \mathcal{O}(g^4), \quad (17)$$

complemented with Eqs. (6) and (9). It is interesting to note that the spatial variable r can be eliminated between Eqs. (14) and (15) to obtain the following nonequilibrium “equation of state”:

$$T = T_0 - \frac{\eta_0}{4\kappa_0} (u_z - u_0)^2 + \mathcal{O}(g^4). \quad (18)$$

By equation of state we mean in this context a relationship holding locally among the hydrodynamic fields (p , u_z and T) and that does not contain g explicitly (at least up to a certain order). Since the pressure is uniform in the NS description, it does not enter into Eq. (18). Equation (18) shows that in the Poiseuille flow the velocity and temperature profiles are closely related.

From Eqs. (13)–(15) we can obtain the mass rate of flow in the NS description. Let us consider a circular section of radius a centered on the cylinder axis and orthogonal to it. The mass of fluid flowing across this surface per unit time is defined, in the reference frame moving with the fluid at $r = a$, as

$$\dot{M}(a) = 2\pi \int_0^a dr r \rho(r) [u_z(r) - u_z(a)]. \quad (19)$$

Using Eqs. (13)–(15) and taking into account that $\rho = mp/k_B T$, one gets

$$\dot{M}(a) = \frac{\pi \rho_0^2 g a^4}{8\eta_0} \left(1 + \frac{5}{384} \frac{\rho_0^2 g^2}{\eta_0 \kappa_0 T_0} a^4 \right) + \mathcal{O}(g^5). \quad (20)$$

Before closing this Section, let us make a few remarks about our use of the term “Navier–Stokes solution”. By that we mean the solution to the coupled set of hydrodynamic equations (10)–(12). In fluid mechanics, on the other hand, it is usual to adopt a more restrictive point of view in which by Navier–Stokes equation one means the momentum equation with a *constant* viscosity η and a constant density ρ (“incompressible fluid”). In that case, the solution of Eq. (11) would simply be

$$u_z(r) = u_0 - \frac{\rho g}{4\eta} r^2, \quad (21)$$

regardless of the value of g . Accordingly, the mass rate of flow would be

$$\dot{M}(a) = \frac{\pi \rho^2 g a^4}{8\eta}. \quad (22)$$

Equation (21) gives the typical parabolic velocity profile under Poiseuille flow, while Eq. (22) is known as Poiseuille’s law [1]. Nevertheless, the shear viscosity η depends in general on the temperature T and so the assumption of a constant viscosity implicitly implies a constant temperature. The same conclusion follows from Eq. (13) and the incompressibility assumption $\rho = \text{const}$. The energy equation (12), however, shows that a velocity profile is compatible with a constant temperature only if the thermal conductivity κ is allowed to be infinite. As a matter of fact, Eqs. (14) and (20) reduce to Eqs. (21) and (22), respectively, if we formally set $\kappa_0 \rightarrow \infty$. Since in a dilute gas the relative strength of the thermal conductivity is comparable to that of the shear viscosity (as measured by the Prandtl number $\text{Pr} \equiv 5k_B \eta / 2m\kappa \simeq \frac{2}{3}$), the energy equation (12) cannot be neglected and hence $T \neq \text{const}$.

In summary, in the remainder of this paper we will refer to Eqs. (10)–(12) as Navier–Stokes equations and will compare their solution for a dilute gas of Maxwell molecules [Eqs. (13)–(15)], along with the momentum and energy fluxes [Eqs. (6), (9), (16) and (17)], with the results derived from the Boltzmann equation.

3 Kinetic theory description

In kinetic theory, the relevant information about the nonequilibrium state of a dilute gas is contained in the one-body distribution function $f(\mathbf{r}, \mathbf{v}; t)$ [20]. Its

temporal evolution is governed by the non-linear Boltzmann equation [18,20], which in standard notation reads

$$\begin{aligned} \frac{\partial}{\partial t} f + \mathbf{v} \cdot \nabla f + \mathbf{g} \cdot \frac{\partial}{\partial \mathbf{v}} f &= \int d\mathbf{v}_1 \int d\Omega |\mathbf{v} - \mathbf{v}_1| \sigma(|\mathbf{v} - \mathbf{v}_1|, \theta) [f' f'_1 - f f_1] \\ &\equiv J[f, f]. \end{aligned} \quad (23)$$

The influence of the interaction potential appears through the dependence of the differential cross section σ on the relative velocity $|\mathbf{v} - \mathbf{v}_1|$ and the scattering angle θ . In particular, for Maxwell molecules $\sigma(|\mathbf{v} - \mathbf{v}_1|, \theta) \propto |\mathbf{v} - \mathbf{v}_1|^{-1}$.

The knowledge of f in a dilute gas is sufficient to determine its macroscopic state. For example, the hydrodynamic variables and their fluxes are just velocity moments of the distribution function. Thus, the local number density n is defined by

$$n = \int d\mathbf{v} f. \quad (24)$$

Analogously, the flow velocity \mathbf{u} and the hydrostatic pressure p are given by the following expressions:

$$\mathbf{u} = \frac{1}{n} \int d\mathbf{v} \mathbf{v} f, \quad (25)$$

$$p = \frac{m}{3} \int d\mathbf{v} V^2 f, \quad (26)$$

where the peculiar velocity $\mathbf{V} = \mathbf{v} - \mathbf{u}$ has been introduced as the velocity of a particle relative to the flow velocity. The momentum and energy fluxes are given by the pressure tensor \mathbf{P} and the heat flux vector \mathbf{q} , respectively, as follows:

$$\mathbf{P} = m \int d\mathbf{v} \mathbf{V} \mathbf{V} f, \quad (27)$$

$$\mathbf{q} = \frac{m}{2} \int d\mathbf{v} V^2 \mathbf{V} f. \quad (28)$$

In the case of the stationary Poiseuille flow in a pipe, the Boltzmann equation (23) becomes

$$v_x \frac{\partial f}{\partial x} + v_y \frac{\partial f}{\partial y} + g \frac{\partial f}{\partial v_z} = J[f, f]. \quad (29)$$

This equation is invariant under the transformations

$$(x, v_x) \longleftrightarrow (-x, -v_x), \quad (y, v_y) \longleftrightarrow (-y, -v_y), \quad (v_z, g) \longleftrightarrow (-v_z, -g). \quad (30)$$

Strictly speaking, Eq. (29) must be supplemented by the appropriate boundary conditions at $r = R$ describing the interaction of the particles with the cylinder surface. However, in this work we are interested in the *bulk* region of the system ($0 < r < R - \delta$, where δ is the width of the boundary layer), which is not affected by the details of the boundary conditions. This implies

that the radius R of the cylinder must be sufficiently large, compared to the mean free path of a particle, to allow the existence of such a region (small Knudsen number). Here we will assume that this is the case and will look for the Hilbert-class or *normal* solution to Eq. (29), namely a solution where all the spatial dependence of the distribution function takes place through a *functional* dependence of f on the hydrodynamic fields n , \mathbf{u} and T .

Since the hydrodynamic variables of the gas and the associated fluxes are the first few moments of the function f , it is convenient to consider the hierarchy of moment equations stemming from the Boltzmann equation (29). A moment of an arbitrary degree $k = k_1 + k_2 + k_3$ is defined as

$$M_{k_1, k_2, k_3}(x, y) = \int d\mathbf{v} V_x^{k_1} V_y^{k_2} V_z^{k_3} f(x, y, \mathbf{v}). \quad (31)$$

The invariance properties (30) imply the parity relations

$$\begin{aligned} M_{k_1, k_2, k_3}(x, y; g) &= (-1)^{k_1} M_{k_1, k_2, k_3}(-x, y; g) \\ &= (-1)^{k_2} M_{k_1, k_2, k_3}(x, -y; g) \\ &= (-1)^{k_3} M_{k_1, k_2, k_3}(x, y; -g). \end{aligned} \quad (32)$$

Although the problem at hand calls for the use of cylindrical coordinates, we will use Cartesian coordinates to construct the moment hierarchy. The reason is two-fold. First, the collision integrals are easier to express in Cartesian (or even spherical) coordinates than in cylindrical coordinates. Second, the use of Cartesian coordinates will serve us as a test of the calculations since, when obtaining the cylindrical components according to Eqs. (A.1) and (A.2), the relevant quantities must depend on x and y through the variable $r = \sqrt{x^2 + y^2}$.

The Boltzmann hierarchy of moments is obtained by multiplying both sides of Eq. (29) by $V_x^{k_1} V_y^{k_2} V_z^{k_3}$ and then integrating over the velocity space. The resulting expression is

$$\begin{aligned} \frac{\partial}{\partial x} M_{k_1+1, k_2, k_3} + \frac{\partial}{\partial y} M_{k_1, k_2+1, k_3} + k_3 \frac{\partial u_z}{\partial x} M_{k_1+1, k_2, k_3-1} + k_3 \frac{\partial u_z}{\partial y} M_{k_1, k_2+1, k_3-1} \\ - g k_3 M_{k_1, k_2, k_3-1} = J_{k_1, k_2, k_3}, \end{aligned} \quad (33)$$

where

$$J_{k_1, k_2, k_3} = \int d\mathbf{v} V_x^{k_1} V_y^{k_2} V_z^{k_3} J[f, f]. \quad (34)$$

In the sequel, we will use the roman boldface \mathbf{k} to denote the triad $\{k_1, k_2, k_3\}$ and the italic lightface k to denote the sum $k_1 + k_2 + k_3$. Thus, $M_{\mathbf{k}} \equiv M_{k_1, k_2, k_3}$ is a moment of degree $k \equiv k_1 + k_2 + k_3$.

The collision integral $J_{\mathbf{k}}$ involves in general all the velocity moments of the distribution (including those of a degree higher than k) and its explicit ex-

pression in terms of those moments is unknown. An important exception is provided by the Maxwell interaction potential $\varphi(r) = K/r^4$. In that case, the collision rate is independent of the velocity, i.e. $|\mathbf{v} - \mathbf{v}_1|\sigma(|\mathbf{v} - \mathbf{v}_1|, \theta) = \sigma_0(\theta)$, and thus $J_{\mathbf{k}}$ can be expressed as a bilinear combination of moments of degree equal to or smaller than k [21,22]:

$$J_{\mathbf{k}} = \sum_{\mathbf{k}', \mathbf{k}''}^{\dagger} C_{\mathbf{k}', \mathbf{k}''}^{\mathbf{k}} M_{\mathbf{k}'} M_{\mathbf{k}''}, \quad (35)$$

where the dagger denotes the constraint $k' + k'' = k$. The coefficients $C_{\mathbf{k}', \mathbf{k}''}^{\mathbf{k}}$ are linear combinations of the eigenvalues [22,23]

$$\lambda_{r\ell} = \int d\Omega \sigma_0(\theta) \left[1 + \delta_{r0}\delta_{\ell 0} - \cos^{2r+\ell} \frac{\theta}{2} P_{\ell} \left(\cos \frac{\theta}{2} \right) - \sin^{2r+\ell} \frac{\theta}{2} P_{\ell} \left(\sin \frac{\theta}{2} \right) \right] \quad (36)$$

of the linearized collision operator, where $P_{\ell}(x)$ are Legendre polynomials. The thermal conductivity and shear viscosity for Maxwell molecules (first obtained by Maxwell himself) are [20]

$$\kappa(T) = \frac{5k_B}{2m} \frac{p}{n\lambda_{11}}, \quad (37)$$

$$\eta(T) = \frac{p}{n\lambda_{02}}, \quad (38)$$

where $\lambda_{02} = \frac{3}{2}\lambda_{11} = 0.436 \times 3\pi\sqrt{2K/m}$. The eigenvalues $\lambda_{r\ell}$ can also be expressed as linear combinations of the integrals [21]

$$A_{2s} = \int d\Omega \sigma_0(\theta) \sin^{2s} \frac{\theta}{2} \cos^{2s} \frac{\theta}{2}. \quad (39)$$

In particular, $\lambda_{02} = 3A_2$, $\lambda_{04} = 7A_2 - \frac{35}{4}A_4$ and $\lambda_{06} = \frac{27}{2}A_2 - \frac{357}{8}A_4 + \frac{231}{8}A_6$. The first few ratios A_{2s}/A_2 are $A_4/A_2 = 0.15778\dots$, $A_6/A_2 = 0.031196\dots$ and $A_8/A_2 = 0.0066540\dots$. The general expression (35) for $J_{\mathbf{k}}$ was elaborated by Truesdell and Muncaster [21], who also give $J_{\mathbf{k}}$ up to $k = 5$. A simplification algorithm for this formula, along with explicit expressions of $J_{\mathbf{k}}$ for $k = 6-8$, has been recently proposed [24].

To simplify the subsequent analysis, it is suitable to use dimensionless quantities. First, let us define an *effective* collision frequency as

$$\nu = n\lambda_{02}. \quad (40)$$

Next, without loss of generality, we choose a reference frame stationary with the flow at $r = 0$, i.e. $u_0 = 0$. Now we introduce the dimensionless variables

$$\begin{aligned} g^* &= v_0^{-1}\nu_0^{-1}g, & u_z^* &= v_0^{-1}u_z, & p^* &= p_0^{-1}p, & T^* &= T_0^{-1}T, \\ M_{\mathbf{k}}^* &= n_0^{-1}v_0^{-k}M_{\mathbf{k}}, & J_{\mathbf{k}}^* &= n_0^{-1}v_0^{-k}\nu_0^{-1}J_{\mathbf{k}}, & \mathbf{r}^* &= \nu_0 v_0^{-1}\mathbf{r}. \end{aligned} \quad (41)$$

In the above expressions, $v_0 = (k_B T_0/m)^{1/2}$ is the thermal velocity and, as in Eqs. (13)–(18), the subscript 0 means that the quantities are evaluated at $r = 0$. The reduced (gravity) acceleration g^* has a clear physical meaning. The quantity $h_0 \equiv v_0^2/g$ is the so-called scale height [25], i.e. the characteristic distance associated with the external (gravity) field. Thus, $g^* = (v_0/\nu_0)/h_0$ represents the ratio between the mean free path and the distance through which a typical particle undergoes the action of \mathbf{g} . While the parameter g^* is a measure of the field strength on the scale of the mean free path, the Froude number

$$\text{Fr} = \frac{v_0^2}{gR} = \frac{h_0}{R} \quad (42)$$

measures the strength on the scale of the radius of the pipe. The relationship between both dimensionless parameters is

$$\text{Fr} = \frac{\text{Kn}}{g^*}, \quad (43)$$

where $\text{Kn} \equiv (v_0/\nu_0)/R$ is the Knudsen number.

The solution of the hierarchy of equations (33) is a very difficult task, even for Maxwell molecules, due to its nonlinear character and the fact that moments of degree k are coupled to the first spatial derivatives of moments of degree $k+1$. On the other hand, we will restrict ourselves to cases where the parameter g^* is weak. This assumption is well justified in most of the practical situations, where values $g^* > 10^{-2}$ would be abnormally large. For instance, in the case of air at room temperature under the action of terrestrial gravity, $g^* \sim 10^{-12}$. Consequently, we can solve the hierarchy (33) by means of a perturbation expansion in powers of g^* , in a similar way as done in other works [6,8,16,26].

4 Expansion in powers of the external force

For the sake of clarity, the asterisks will be dropped in this Section, so all the quantities will be understood to be expressed in reduced units [cf. Eqs. (41)], unless stated otherwise.

Before performing the power series expansion of the moments, it is convenient to take into account the symmetry properties (32). For example, it is obvious that the profiles of the temperature and the hydrostatic pressure are even functions of g , while the flow velocity u_z is an odd function. Therefore, we can write

$$p = 1 + p^{(2)}g^2 + p^{(4)}g^4 + \dots, \quad (44)$$

$$T = 1 + T^{(2)}g^2 + T^{(4)}g^4 + \dots, \quad (45)$$

$$u_z = u^{(1)}g + u^{(3)}g^3 + \dots . \quad (46)$$

The expansion of the number density $n = M_{000} = p/T$ can be obtained from Eqs. (44) and (45). These hydrodynamic fields are (even) functions of x and y through the distance $r = \sqrt{x^2 + y^2}$. As for the moments $M_{\mathbf{k}}$, they are even (odd) functions of g if their index k_3 is even (odd). Thus,

$$M_{\mathbf{k}} = M_{\mathbf{k}}^{(0)} + M_{\mathbf{k}}^{(1)}g + M_{\mathbf{k}}^{(2)}g^2 + M_{\mathbf{k}}^{(3)}g^3 + \dots , \quad (47)$$

where $M_{\mathbf{k}}^{(s)} = 0$ if $s + k_3 = \text{odd}$. The zeroth-order term $M_{\mathbf{k}}^{(0)}$ is the moment of the equilibrium distribution function normalized to $p^{(0)} = 1$, $T^{(0)} = 1$. Its expression is

$$M_{\mathbf{k}}^{(0)} = C_{k_1} C_{k_2} C_{k_3}, \quad (48)$$

where $C_k = (k-1)!! = (k-1) \times (k-3) \times (k-5) \times \dots \times 1$ if $k = \text{even}$, being 0 if $k = \text{odd}$.

In the first stage of the calculations, the expansions (44)–(47) are inserted into Eq. (33). By equating the terms of degree s in g on both sides, we get

$$\begin{aligned} \frac{\partial}{\partial x} M_{k_1+1, k_2, k_3}^{(s)} + \frac{\partial}{\partial y} M_{k_1, k_2+1, k_3}^{(s)} + k_3 \sum_{i=0}^{[(s-1)/2]} \left[\frac{\partial u^{(2i+1)}}{\partial x} M_{k_1+1, k_2, k_3-1}^{(s-1-2i)} \right. \\ \left. + \frac{\partial u^{(2i+1)}}{\partial y} M_{k_1, k_2+1, k_3-1}^{(s-1-2i)} \right] - k_3 M_{k_1, k_2, k_3-1}^{(s-1)} = J_{\mathbf{k}}^{(s)}, \end{aligned} \quad (49)$$

where $[\alpha]$ means the integer part of α . According to Eq. (35), the right side of (49) is

$$J_{\mathbf{k}}^{(s)} = \sum_{\mathbf{k}', \mathbf{k}''} \dagger C_{\mathbf{k}', \mathbf{k}''}^{\mathbf{k}} \sum_{i=0}^s M_{\mathbf{k}'}^{(s-i)} M_{\mathbf{k}''}^{(i)}. \quad (50)$$

Equation (50) is still very difficult to solve in general. First, it is nonlinear and couples moments of degree k and lower to moments of degree $k+1$. Second, the coefficients $M_{\mathbf{k}}^{(s)}$ are unknown functions of the spatial variables x and y . To overcome the latter obstacle, we assume that a self-consistent solution of Eq. (49) exists in which the coefficients in the series defined by (44)–(47) are *polynomials* in x and y . This ansatz is justified by the results obtained in the case of the planar geometry from the BGK model [6] and the Boltzmann equation [8], as well as in the case of the cylindrical geometry from the BGK model [16]. More specifically, we assume that the coefficients of the hydrodynamic profiles are of the form

$$p^{(s)} = \sum_{i=1}^{s-1} p_{2i}^{(s)} r^{2i}, \quad (51)$$

$$T^{(s)} = \sum_{i=1}^s T_{2i}^{(s)} r^{2i}, \quad (52)$$

$$u^{(s)} = \sum_{i=1}^s u_{2i}^{(s)} r^{2i}. \quad (53)$$

The task becomes more difficult when guessing the spatial dependence of the coefficients $M_{\mathbf{k}}^{(s)}$. It can be checked that the only representation that leads to consistent solutions of the hierarchy (49) is of the form

$$M_{\mathbf{k}}^{(s)} = \sum_{i=0}^{\sigma(s)} \sum_{j=0}^i \chi_{\mathbf{k}}^{(s,i-j,j)} x^{i-j} y^j, \quad (54)$$

where $\sigma(s=1) = 1$ and $\sigma(s) = 2s$ for $s > 1$. From Eqs. (32) it follows that $\chi_{k_1, k_2, k_3}^{(s,i,j)} = 0$ if $s + k_3 = \text{odd}$ or $i + k_1 = \text{odd}$ or $j + k_2 = \text{odd}$. Insertion of Eq. (54) into Eq. (50) shows that $J_{\mathbf{k}}^{(s)}$ has the same structure as $M_{\mathbf{k}}^{(s)}$, namely

$$J_{\mathbf{k}}^{(s)} = \sum_{i=0}^{\sigma(s)} \sum_{j=0}^i J_{\mathbf{k}}^{(s,i-j,j)} x^{i-j} y^j. \quad (55)$$

The numerical coefficients $p_{2i}^{(s)}$, $T_{2i}^{(s)}$, $u_{2i}^{(s)}$ and $\chi_{\mathbf{k}}^{(s,i,j)}$ are determined by consistency. To do so, we insert Eqs. (51)–(54) into Eq. (49) and equate the coefficients of the terms $x^i y^j$ in both sides. This yields a hierarchy of *linear* equations for the unknowns. In the hierarchy, the coefficients of the moments of degree $k+1$, k and $k-1$ on the left-hand side are related to those of degree k , $k-1$, $k-2$, \dots on the right-hand side. In addition, the coefficients of the type $\chi_{k_1+1, k_2, k_3}^{(s,i+1,j)}$ and $\chi_{k_1, k_2+1, k_3}^{(s,i,j+1)}$ on the left-hand side determine those of the type $\chi_{k_1, k_2, k_3}^{(s,i,j)}$ on the right-hand side. In spite of the intricacy of the resulting hierarchy, it can be recursively solved by following steps similar to those made in the case of the planar geometry [8]. To get explicit results to order $s=3$ it is necessary to consider the moment equations up to degree $k=8$.

The method is outlined in Appendix B and the main results are presented in the next Section.

5 Discussion

5.1 Hydrodynamic profiles

By proceeding along the recursive scheme described in Appendix B, we have obtained the explicit spatial dependence of the coefficients in the series ex-

pansions (44)–(46) through order g^4 and those of the series expansion (47) for moments of second ($k = 2$) and third ($k = 3$) degrees through order g^3 . Here we display the results to third order. Also, to ease the physical interpretation of the results, they are expressed in cylindrical coordinates and in real units. The hydrodynamic profiles are

$$u_z(r) = u_0 - \frac{\rho_0 r^2 g}{4\eta_0} \left[1 + \frac{1}{144} \frac{\rho_0^2 g^2}{\kappa_0 \eta_0 T_0} r^4 + \zeta_u \left(\frac{mg}{k_B T_0} \right)^2 r^2 + \zeta'_u \frac{\rho_0 \eta_0^2 g^2}{p_0^3} \right] + \mathcal{O}(g^5), \quad (56)$$

$$p(r) = p_0 \left[1 + \zeta_p \left(\frac{mg}{k_B T_0} \right)^2 r^2 \right] + \mathcal{O}(g^4), \quad (57)$$

$$T(r) = T_0 \left[1 - \frac{1}{64} \frac{\rho_0^2 g^2}{\kappa_0 \eta_0 T_0} r^4 + \zeta_T \left(\frac{mg}{k_B T_0} \right)^2 r^2 \right] + \mathcal{O}(g^4), \quad (58)$$

where $\zeta_u = \frac{4429}{12600} \simeq 0.35$, $\zeta'_u = 24.322\dots$, $\zeta_p = \frac{3}{10}$ and $\zeta_T = \frac{34}{175} \simeq 0.19$. We recall that the subscript 0 in a quantity represents its value on the z -axis, i.e. at $r = 0$. Elimination of r among Eqs. (56)–(58) allows one to get the following nonequilibrium equation of state:

$$T = T_0 - \frac{\eta_0}{4\kappa_0} (u_z - u_0)^2 + \frac{\zeta_T T_0}{\zeta_p p_0} (p - p_0) + \mathcal{O}(g^4). \quad (59)$$

The non-zero elements of the pressure tensor are

$$P_{rr}(r) = p_0 \left[1 + \frac{1}{6} \zeta_p \left(\frac{mg}{k_B T_0} \right)^2 r^2 - \zeta'_P \frac{\rho_0 \eta_0^2 g^2}{p_0^3} \right] + \mathcal{O}(g^4), \quad (60)$$

$$P_{\phi\phi}(r) = p_0 \left[1 + \frac{1}{2} \zeta_p \left(\frac{mg}{k_B T_0} \right)^2 r^2 - \zeta'_P \frac{\rho_0 \eta_0^2 g^2}{p_0^3} \right] + \mathcal{O}(g^4), \quad (61)$$

$$P_{zz}(r) = p_0 \left[1 + \frac{7}{3} \zeta_p \left(\frac{mg}{k_B T_0} \right)^2 r^2 + 2\zeta'_P \frac{\rho_0 \eta_0^2 g^2}{p_0^3} \right] + \mathcal{O}(g^4), \quad (62)$$

$$P_{rz}(r) = \frac{\rho_0 g}{2} r \left[1 + \frac{1}{192} \frac{\rho_0^2 g^2}{\kappa_0 \eta_0 T_0} r^4 + \frac{\zeta_p - \zeta_T}{2} \left(\frac{mg}{k_B T_0} \right)^2 r^2 \right] + \mathcal{O}(g^5), \quad (63)$$

where $\zeta'_P = 1.7388\dots$. Finally, the components of the heat flux are

$$q_r(r) = \frac{1}{16} \frac{\rho_0^2 g^2}{\eta_0} r^3 + \mathcal{O}(g^4), \quad (64)$$

$$q_z(r) = -\frac{2}{5} \frac{\kappa_0 mg}{k_B} \left[\zeta_0 - \zeta_q \frac{\rho_0^2 g^2}{\kappa_0 \eta_0 T_0} r^4 - \zeta'_q \left(\frac{mg}{k_B T_0} \right)^2 r^2 - \zeta''_q \frac{\rho_0 \eta_0^2 g^2}{p_0^3} \right] + \mathcal{O}(g^5), \quad (65)$$

where $\zeta_0 = 1$, $\zeta_q = \frac{37}{28} \simeq 0.29$, $\zeta'_q = 3.2527 \dots$ and $\zeta''_q = 86.415 \dots$

Equations (56)–(65) are the main results of this paper. They give the *exact* profiles in the bulk region of the hydrodynamic fields and their fluxes for a dilute gas of Maxwell molecules through third order in the external force. Comparison of Eqs. (6), (9) and (13)–(18) with Eqs. (56)–(65) show that the NS constitutive equations predict $\zeta_u = \zeta'_u = \zeta_p = \zeta_T = \zeta'_P = \zeta_0 = \zeta_q = \zeta'_q = \zeta''_q = 0$. These vanishing values of the coefficients summarize the main limitations of the NS description of the Poiseuille flow induced by an external force. Equation (65) shows that $q_z \neq 0$, even to first order in g ($\zeta_0 \neq 0$), despite the absence of a thermal gradient along the longitudinal direction. This represents an obvious breakdown of Fourier's law and is in fact a Burnett-order effect [8]. To second order in g the hydrostatic pressure is not uniform but increases radially ($\zeta_p > 0$); analogously, there are normal stress differences, so that $P_{rr} < P_{\phi\phi} < p < P_{zz}$. These are non-Newtonian effects.

Also to second order in g , there exists a positive quadratic term ($\zeta_T > 0$) in addition to the negative quartic term in the temperature profile. The former term is responsible for the fact that the temperature has a local minimum rather than a maximum at $r = 0$. The maximum temperature is located at a distance $r_{\max} = \sqrt{32\zeta_T}\ell_0 \simeq 2.49\ell_0$ (independent of g), where $\ell_0 \equiv (\eta_0\kappa_0T_0)^{1/2}/p_0 = \sqrt{\frac{2}{5}}\text{Pr}(v_0/\nu_0)$ is the (local) mean free path at $r = 0$; the relative difference between the maximum temperature and the temperature on the cylinder axis is $(T_{\max} - T_0)/T_0 = 16\zeta_T^2(\ell_0/h_0)^2 \simeq 0.604(\ell_0/h_0)^2$, where we recall that $h_0 \equiv k_B T_0/mg$. This result represents a dramatic violation of Fourier's law: while the heat flows radially outwards, the temperature increases from $r = 0$ to $r = r_{\max}$. Therefore, within the region $0 \leq r \leq r_{\max}$, the heat flows from the colder to the hotter layers. This paradoxical effect, which is beyond the Burnett description [11], does not violate the conservation of energy (5) since the radial increase of rq_r (which tends to cool the gas) is exactly compensated for by the viscous heating term $rP_{rz}\partial u_z/\partial r$. It is interesting to note that from Eqs. (58) and (64) one can obtain

$$-\kappa \frac{\partial T}{\partial r} = q_r - \frac{1}{9}r_{\max}^2 \nabla^2 q_r + \mathcal{O}(g^4), \quad (66)$$

where $\nabla^2 X = r^{-1}\partial(r\partial X/\partial r)/\partial r$ is the Laplacian in cylindrical coordinates. Equation (66) is an extension of Fourier's law (8) showing that the sign of the thermal gradient results from a competition between the radial component of the heat flux and its Laplacian [10]. The latter dominates for $r < r_{\max}$ and so $\partial T/\partial r > 0$ in that region.

Third-order contributions appear in u_z and P_{rz} but they do not have a qualitatively important influence. They are responsible for a spatial variation of the flow velocity u_z and the shear stress P_{rz} more pronounced than expected from the NS equations. The same happens for the mass rate of flow defined

by Eq. (19). Insertion of the hydrodynamic profiles (56)–(58) yields

$$\dot{M}(a) = \frac{\pi \rho_0^2 g a^4}{8 \eta_0} \left[1 + \frac{5}{384} \frac{\rho_0^2 g^2}{\eta_0 \kappa_0 T_0} a^4 + \frac{4\zeta_u + \zeta_p - \zeta_T}{3} \left(\frac{mg}{k_B T_0} \right)^2 a^2 + \zeta'_u \frac{\rho_0 \eta_0^2 g^2}{p_0^3} \right] + \mathcal{O}(g^5). \quad (67)$$

Comparison with Eq. (20) shows that the mass rate of flow grows with the radius a more rapidly than predicted by the NS approximation, but otherwise the qualitative behavior is similar in both descriptions.

5.2 Generalized constitutive equations

Let us use Eqs. (56)–(65) to rewrite the fluxes under the form of *generalized* constitutive equations. We begin with the shear stress:

$$P_{rz} = -\eta \frac{\partial u_z}{\partial r} \left[1 - \frac{\zeta'_u}{15\zeta_T} \frac{\ell^2}{T} \nabla^2 T - \frac{4}{15} \left(\frac{\zeta'_u}{15\zeta_T} + 8\zeta_u + 6\zeta_T - 2\zeta_p \right) \times \frac{\ell^2}{k_B T/m} \left(\frac{\partial u_z}{\partial r} \right)^2 \right] + \mathcal{O}(g^5). \quad (68)$$

Here $\eta \propto T$ is the local shear viscosity at r , so $\eta - \eta_0 \propto T - T_0 = \mathcal{O}(g^2)$. Analogously, $\ell = (\eta \kappa T)^{1/2} / p$ is the local mean free path and $\ell - \ell_0 = \mathcal{O}(g^2)$. In Eq. (68) the NS term is of order g , while the super-Burnett terms (i.e. of third order in the hydrodynamic gradients) are of order g^3 . The normal stresses can be written as

$$P_{rr} = p \left[1 + \frac{10\zeta_p}{3} \frac{\ell^2}{T} \nabla^2 T - \left(\frac{\zeta'_p}{15\zeta_p} + \frac{10\zeta_T}{3} \right) \frac{\ell^2}{p} \nabla^2 p \right] + \mathcal{O}(g^4), \quad (69)$$

$$P_{\phi\phi} = p \left[1 + 2\zeta_p \frac{\ell^2}{T} \nabla^2 T - \left(\frac{\zeta'_p}{15\zeta_p} + 2\zeta_T \right) \frac{\ell^2}{p} \nabla^2 p \right] + \mathcal{O}(g^4), \quad (70)$$

$$P_{zz} = p \left[1 - \frac{16\zeta_p}{3} \frac{\ell^2}{T} \nabla^2 T + \left(\frac{2\zeta'_p}{15\zeta_p} + \frac{16\zeta_T}{3} \right) \frac{\ell^2}{p} \nabla^2 p \right] + \mathcal{O}(g^4). \quad (71)$$

Thus, in order to obtain the normal stresses to order g^2 we need to include at least the Burnett contributions in the Chapman–Enskog expansion.

The radial component of the heat flux can be expressed as

$$q_r = -\kappa \frac{\partial}{\partial r} \left(T + 4\zeta_T \ell^2 \nabla^2 T \right) + \mathcal{O}(g^4). \quad (72)$$

In this case, both the NS term and the super-Burnett term are of order g^2 . As for the longitudinal heat flux, one has

$$q_z = \frac{\eta^2}{2\rho} (\nabla^2 u_z) \left(\theta_4 - \frac{\zeta'_u + \zeta''_q}{5\zeta_T} \nabla^2 T \right) + \frac{2}{5} n k_B \ell^2 \frac{\partial u_z}{\partial r} \times \left(\theta_5 \frac{\partial T}{\partial r} + \frac{\theta_3 T}{3 p} \frac{\partial p}{\partial r} + \mu \ell^2 \frac{\partial}{\partial r} \nabla^2 T \right) + \mathcal{O}(g^5), \quad (73)$$

where $\theta_3 = -3$, $\theta_4 = 3\zeta_0 = 3$, $\theta_5 = \frac{1}{2}(1 + 64\zeta_q) = \frac{39}{4}$ and

$$\mu = \frac{\zeta'_u + \zeta''_q}{15\zeta_T} + 16\zeta_u + 2\zeta_T(7 + 64\zeta_q) + 4\zeta'_q - 8\zeta_p \simeq 64.141 \dots \quad (74)$$

The Burnett term headed by θ_4 is of first order in g , while the Burnett terms with θ_3 and θ_5 are of third order. In addition, there are super-super-Burnett terms that are also of order g^3 .

Equations (68)–(73) can be written in other equivalent forms by taking into account that the hydrodynamic gradients are not independent in our problem. For instance,

$$\frac{m}{k_B T} \left(\frac{\partial u_z}{\partial r} \right)^2 = \frac{15}{4} \left(\frac{\zeta_T}{\zeta_p} \frac{1}{p} \nabla^2 p - \frac{1}{T} \nabla^2 T \right) + \mathcal{O}(g^4), \quad (75)$$

$$\nabla^2 p = -4\zeta_p \frac{p}{T} \ell^2 \nabla^4 T + \mathcal{O}(g^4) = \frac{16}{15} \zeta_p \frac{mp}{k_B T} \ell^2 (\nabla^2 u_z)^2 + \mathcal{O}(g^4). \quad (76)$$

In particular, Eq. (76) implies that the Burnett term $\nabla^2 p$ and the super-super-Burnett terms $\nabla^4 T$ and $(\nabla^2 u_z)^2$ are of order g^2 . Therefore, in order to obtain correctly the profiles (56)–(65) from the Chapman–Enskog method one would actually need to go beyond the apparent orders in the gradients of Eqs. (68)–(73).

The previous analysis shows that the Chapman–Enskog expansion and the expansion in powers of g in the Poiseuille flow are quite different, even though the gradients are induced by the external force. Both expansions require a weak field, namely $h_0 \gg \ell_0$. On the other hand, while the Chapman–Enskog expansion requires that $\ell_0^2 T_0^{-1} \nabla^2 T \ll 1$, i.e. $r \gg \ell_0$, the expansion in powers of g remains valid for distances smaller than or of the order of the mean free path. Since the non-monotonic behavior of the temperature profile occurs for $0 \leq r \leq r_{\max} \sim \ell_0$, this effect is neglected by the NS description.

Table 1

Numerical values of the coefficients appearing in Eqs. (56)–(65), as obtained from the Boltzmann equation for Maxwell molecules (BM) and for from the BGK model for Maxwell molecules. The ratio between the BM and BGK values are displayed in the third column.

ζ	BM	BGK	BM/BGK
ζ_u	$\frac{4429}{12600}$	$\frac{89}{200}$	0.79
ζ'_u	24.322	64	0.38
ζ_p	$\frac{3}{10}$	$\frac{3}{10}$	1
ζ_T	$\frac{34}{175}$	$\frac{7}{50}$	1.38
ζ'_P	1.7388	$\frac{92}{25}$	0.47
ζ_0	1	1	1
ζ_q	$\frac{37}{128}$	$\frac{15}{64}$	1.23
ζ'_q	3.2527	$\frac{209}{50}$	0.78
ζ''_q	86.415	$\frac{5432}{25}$	0.39

5.3 Comparison with the BGK solution

Once we have discussed the limits of validity of the NS theory (which otherwise provides a powerful tool to study the macroscopic state of many nonequilibrium flows) in our Poiseuille problem, it is worthwhile wondering whether the BGK model kinetic equation succeeds in capturing the main qualitative features of the Boltzmann solution. The solution of the BGK model for the cylindrical Poiseuille flow was obtained by Tij and Santos [16] to fourth order in g for a general class of power-law repulsive potentials. The results agree exactly with the structure of Eqs. (56)–(65). On the other hand, most of the coefficients ζ 's have different numerical values. The failure of the BGK model to reproduce the exact Boltzmann values for those coefficients is not surprising, given the simplicity of the model, which assumes that the practical effect of collisions is to make the distribution function relax to local equilibrium with a single characteristic rate ν . In fact, it is well known [18] that the BGK model yields a value ($\text{Pr} = 1$) for the Prandtl number $\text{Pr} \equiv 5k_B\eta/2m\kappa$ different from the correct one ($\text{Pr} = \frac{2}{3}$). Table 1 compares the numerical values of the coefficients ζ 's given by the Boltzmann equation for Maxwell molecules (BM) with those obtained from the BGK model. Except for ζ_p and ζ_0 , the coefficients are different in both theories, the ratio being bounded between 0.38 and 1.38. For instance, the location r_{\max} of the maximum temperature is in the BGK model 15% smaller than in the Boltzmann equation and the temperature difference $T_{\max} - T_0$ in the BGK model is almost half the Boltzmann value. A comparison of the coefficients appearing in the hydrodynamic fields to fourth order in g [not shown in Eqs. (57) and (58), but given in Appendix B] shows that the

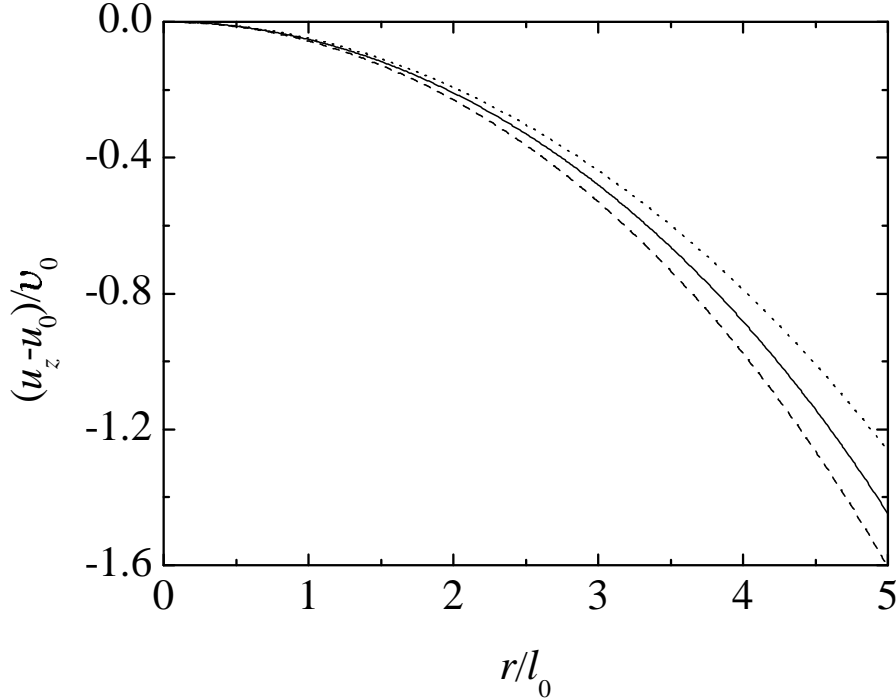


Fig. 1. Profile of the flow velocity $u_z(r)$ for $g = 0.1v_0^2/\ell_0$, as obtained from the Navier–Stokes (NS) equations (dotted line), the Boltzmann equation for Maxwell molecules (BM) (solid line) and the BGK model (dashed line).

discrepancies between the BGK and Boltzmann equations increase with the power of g . In particular, the series obtained from the BGK model seem to diverge more quickly than those obtained from the Boltzmann equation.

In order to illustrate graphically the differences between the NS, BGK and BM descriptions, we plot in Figs. 1–6 the hydrodynamic and flux profiles for the case $g = 0.1v_0^2/\ell_0$ [which corresponds to $h_0/\ell_0 = 10$], when only terms through third order in g are retained. Of course, higher order terms are not expected to be negligible for that particular high value of the external field [27], especially as one departs from the axis, as discussed in Subsection 5.5. However, the retained terms are sufficient to show the qualitative differences in the predictions of the three approaches, so that the main aim of Figs. 1–6 is to highlight those differences. It must be born in mind that the BGK curves in Figs. 1–6 correspond to Eqs. (56)–(65) with the BGK values for the coefficients ζ 's (cf. Table 1) but with the correct value $\text{Pr} = \frac{2}{3}$ of the Prandtl number. As expected, the BGK model is in qualitative agreement with the BM results.

5.4 Comparison with the planar Poiseuille flow

Let us now add a few comments on the similarities between the cylindrical and the planar Poiseuille flows. The solution of the Boltzmann equation for

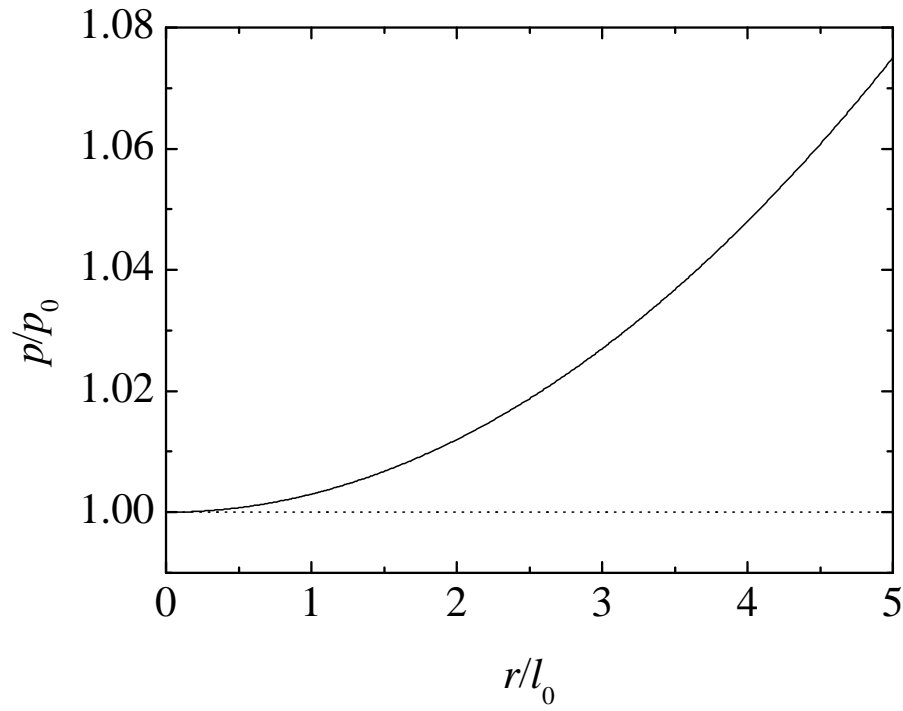


Fig. 2. Same as in Fig. 1, but for the hydrostatic pressure $p(r)$. Note that the BM and BGK curves coincide.

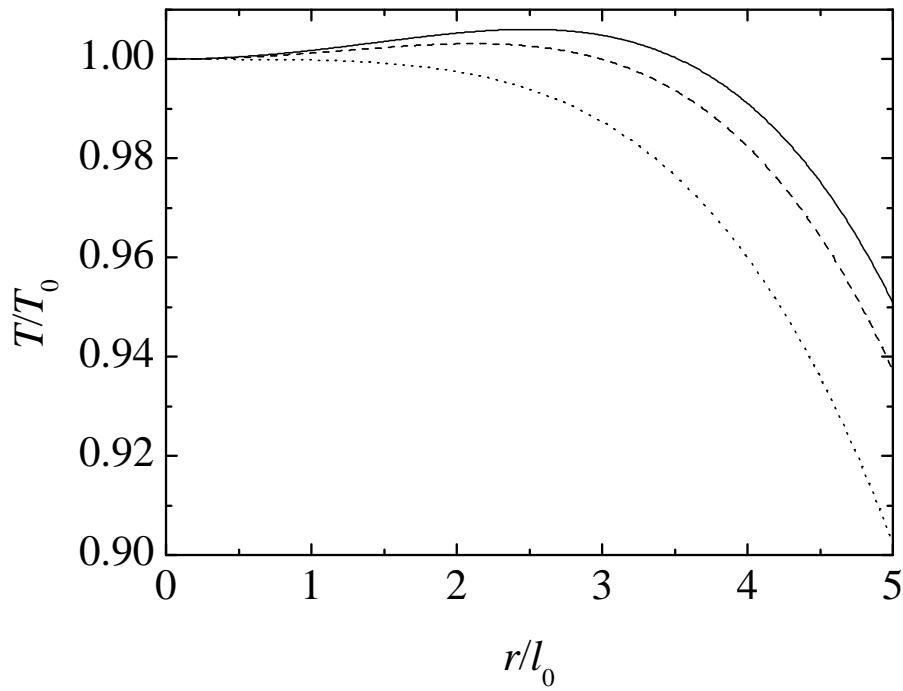


Fig. 3. Same as in Fig. 1, but for the temperature $T(r)$.

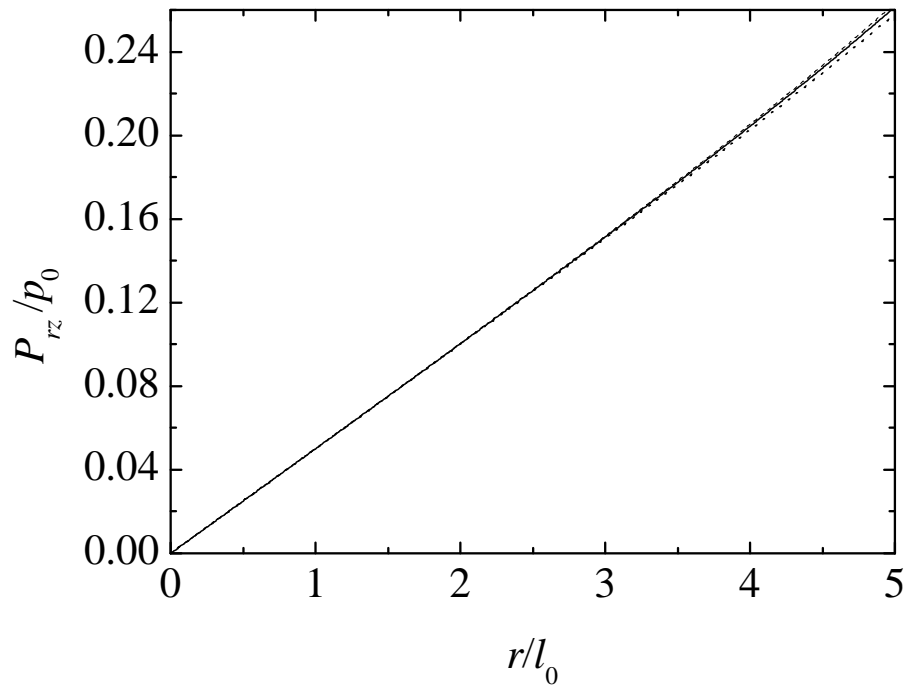


Fig. 4. Same as in Fig. 1, but for the shear stress $P_{rz}(r)$. The NS and BGK curves are slightly below and above, respectively, the BM curve.

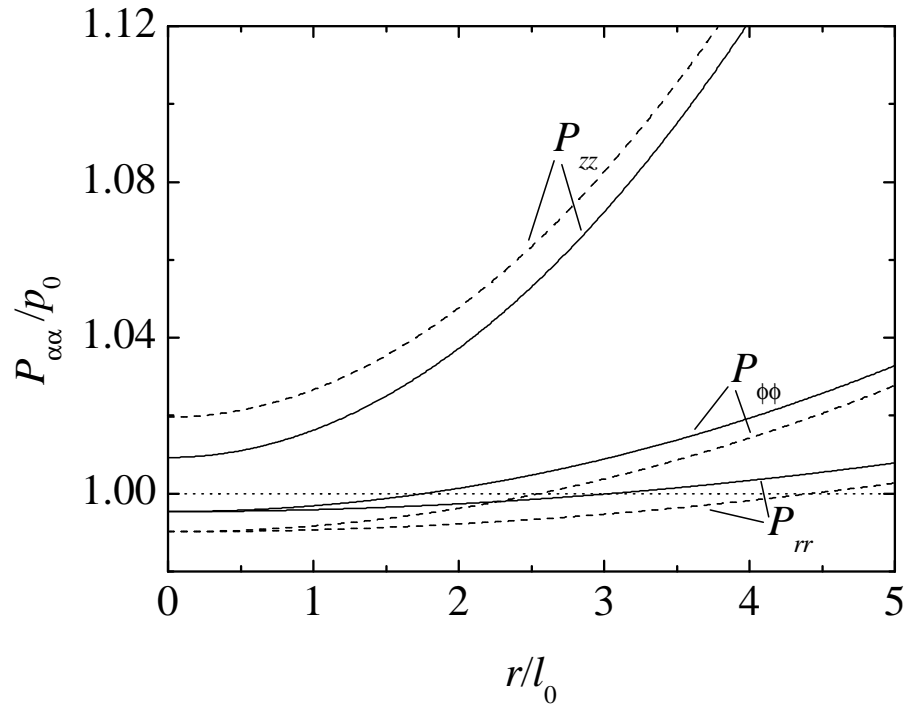


Fig. 5. Same as in Fig. 1, but for the normal stresses $P_{rr}(r)$, $P_{\phi\phi}(r)$ and $P_{zz}(r)$. Note that in the NS approximation $P_{rr} = P_{\phi\phi} = P_{zz} = p$.

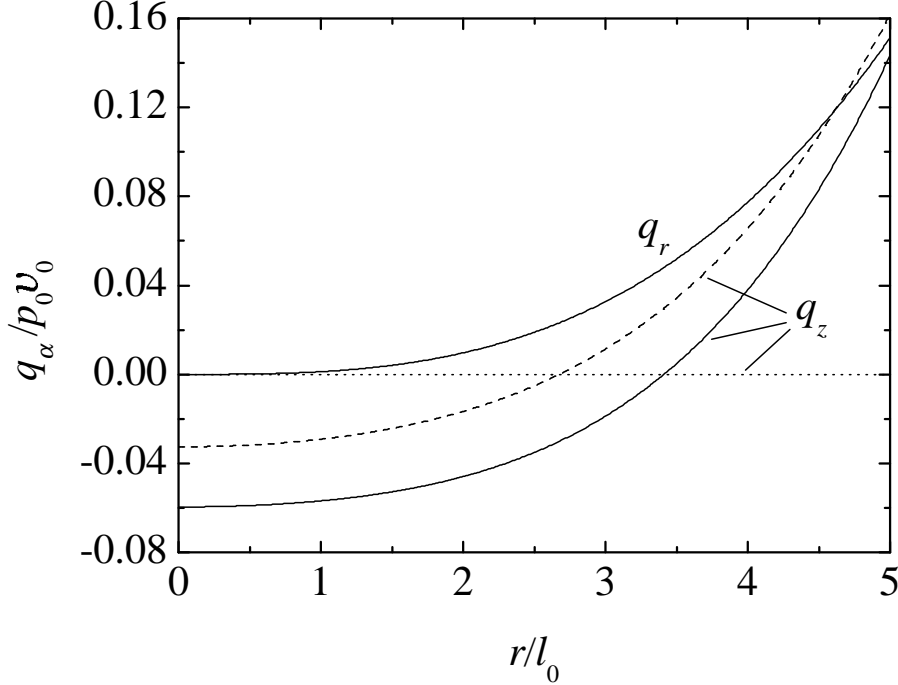


Fig. 6. Same as in Fig. 1, but for the components of the heat flux. Note that the NS, BM and BGK curves coincide for the radial component $q_r(r)$.

Maxwell molecules to order g^2 in the planar geometry [8] yields profiles analogous to those of Eqs. (56)–(65). In particular, the temperature profile is

$$T(y) = T_0 \left[1 - \frac{1}{12} \frac{\rho_0^2 g^2}{\kappa_0 \eta_0 T_0} y^4 + \zeta_T \left(\frac{mg}{k_B T_0} \right)^2 y^2 \right] + \mathcal{O}(g^4), \quad (77)$$

where now $\zeta_T = 1.0153$. As a consequence, the temperature has a maximum with $(T_{\max} - T_0)/T_0 = 3\zeta_T^2(\ell_0/h_0)^2 \simeq 3.09(\ell_0/h_0)^2$ at $|y| = y_{\max} = \sqrt{6\zeta_T}\ell_0 \simeq 2.47\ell_0$. Therefore, the maximum temperature occurs at a separation y_{\max} from the middle plane practically equal to the radial distance r_{\max} of the cylindrical case, but the relative temperature change $(T_{\max} - T_0)/T_0$ is about five times larger in the former case than in the latter. Interestingly, this effect is accurately captured by the BGK model [16], as explained by the fact that in the planar Poiseuille flow one has [6,8] $\zeta_p^{\text{BM}}/\zeta_p^{\text{BGK}} = 1$, $\zeta_T^{\text{BM}}/\zeta_T^{\text{BGK}} = 1.0153/(19/25) \simeq 1.34$, $\zeta_P^{\text{BM}}/\zeta_P^{\text{BGK}} = 6.2602/(306/25) \simeq 0.51$, $\zeta_0^{\text{BM}}/\zeta_0^{\text{BBGK}} = 1$, in close agreement with the corresponding ratios in the cylindrical Poiseuille flow (see Table 1).

5.5 Boundary conditions

When solving the Boltzmann hierarchy of moments [cf. Eq. (33)] by a perturbation expansion in powers of gravity we have taken the hydrodynamic

quantities at the axis ($r = 0$) as reference values. In so doing, we have avoided the need of imposing specific boundary conditions. The price to be paid is that it is difficult to determine how far from the axis the profiles (56)–(65) remain valid. Consider for instance the temperature profile (58). The first neglected term $\mathcal{O}(g^4)$ is a polynomial in r of degree 8 [cf. Eq. (B.19)]. This term can actually be neglected versus the retained terms only if $g^{*4}(r/\ell_0)^8 \ll g^{*2}(r/\ell_0)^4$, i.e. if

$$g^*(r/\ell_0)^2 \ll 1. \quad (78)$$

The same conclusion is obtained from the velocity profile (56) and the pressure profile (57). If $r \sim \ell_0$, condition (78) is equivalent to $g^* \ll 1$. On the other hand, a much stronger condition $g^* \ll \text{Kn}^2$ is needed to extend the profiles (56)–(65) to distances r comparable with the pipe radius R . In order to find the hydrodynamic fields for $r \sim R$ when condition (78) does not hold, one would need to solve the full Boltzmann equation with the appropriate (e.g. diffuse reflection) boundary conditions at $r = R$ corresponding to a given wall temperature T_w . This has been done by Aoki et al. [12] in the case of the BGK equation for the planar geometry. They derived the hydrodynamic equations and the matching conditions corresponding to the normal (or Hilbert) solution by an asymptotic expansion in powers of the Knudsen number Kn and for values of the Froude number of order $\text{Fr} \sim 1/\text{Kn}$. In view of Eq. (43), this implies that $g^* \sim \text{Kn}^2$. The successive hydrodynamic equations had to be solved numerically, but Aoki et al. verified that a Taylor series expansion around the center of the gap agreed with the perturbation solution found in Ref. [6].

An asymptotic method analogous to that worked out by Aoki et al. [12] would be much more difficult to carry out in the case of the Boltzmann equation for the cylindrical geometry. Nevertheless, it is natural to expect that the results derived in this paper would be recovered by performing a Taylor series expansion around $r = 0$ of the solution for $g^* \sim \text{Kn}^2$. This in addition would provide the matching conditions for the profiles (56)–(58) in the region $r/\ell_0 \sim g^{*-1/2} \sim \text{Kn}^{-1}$.

6 Conclusion

In this work, we have studied the (laminar) stationary Poiseuille flow in a cylindrical pipe induced by an external force $m\mathbf{g}$. We have considered a dilute gas of Maxwell molecules and have analyzed the hierarchy of moment equations associated with the nonlinear Boltzmann equation. A consistent solution has been found under the form of a perturbation expansion in powers of g through third order. In principle, the method can be pushed to higher orders but, not only the algebraic intricacy of the solution scheme grows rapidly,

but the results would not be of practical use given the suspected asymptotic character of the series. The discussion of the results has focused on the most relevant physical quantities, namely the hydrodynamic profiles (flow velocity, pressure and temperature) and the associated fluxes (pressure tensor and heat flux). The results obtained here show once again that the Navier–Stokes (NS) theory remains unable to envisage the correct hydrodynamic profiles, even at a qualitative level, for distances smaller than or of the order of the mean free path. The most important limitation of the NS description is that it predicts a monotonically decreasing temperature as one moves apart from the cylinder axis. In contrast, our solution to the Boltzmann equation shows that the temperature has a local minimum ($T = T_0$) at the axis ($r = 0$) and reaches a maximum value $T = T_{\max} \simeq T_0 [1 + 0.6(\ell_0/h_0)^2]$ at a distance from the center $r = r_{\max} \simeq 2.5\ell_0$ of the order of the mean free path ℓ_0 . In addition, a longitudinal component of the heat flux exists ($q_z \neq 0$) in the absence of gradients along the longitudinal direction and normal stress differences ($P_{rr} < P_{\phi\phi} < p < P_{zz}$) are present. On the other hand, the BGK model provides results qualitatively similar to those found in this paper [16]. Notwithstanding this, the profiles predicted by the BGK model require some corrections from a quantitative point of view, as expected. In particular, the BGK model underestimates the maximum value T_{\max} of the temperature, as well as its location r_{\max} . From that point of view, one might say that the BGK model deviates from the NS predictions less than the Boltzmann equation, at least for Maxwell molecules. The same conclusion arises from a comparison between the Boltzmann and BGK results for the planar Poiseuille flow [6,8]. Nevertheless, it is worth noting that the BGK model is accurate in describing the effect of the geometry of the Poiseuille flow on the profiles. For instance, it correctly predicts that in the planar case the maximum temperature is located at a separation y_{\max} from the middle plane practically equal to the radial distance r_{\max} of the cylindrical case, although the relative temperature change $(T_{\max} - T_0)/T_0$ is about five times larger in the former case than in the latter.

Although we have not considered interactions different from Maxwell’s, we expect the results found here to remain essentially valid, except that the numerical values of the coefficients may change. This expectation is supported by the results obtained with the BGK kinetic model [16]. In that case one finds that the coefficients ζ_p , ζ_T , ζ'_P and ζ_0 are universal, while the coefficients ζ_u , ζ'_u , ζ_q , ζ'_q and ζ''_q change by 5%, 0.5%, 3%, 0.7% and 0.8%, respectively, when going from Maxwell molecules to hard spheres.

Let us conclude by asserting that the stationary Poiseuille flow driven by an external force, both in a slab and in a pipe, is a good and conceptually simple example in fluid dynamics showing the limitations of a purely continuum theory in contrast to a kinetic theory approach. Next, we want to emphasize the important role played by the BGK model kinetic equation to pave the way towards a more fundamental theory based on the Boltzmann equation.

Acknowledgements

A.S. gratefully acknowledges partial support from the Ministerio de Ciencia y Tecnología (Spain) through grant No. BFM2001-0718.

A Cylindrical coordinates

The relationships between the cylindrical and Cartesian components of a vector \mathbf{A} and a tensor \mathbf{B} are

$$\begin{pmatrix} A_r \\ A_\phi \\ A_z \end{pmatrix} = \mathbf{U} \cdot \begin{pmatrix} A_x \\ A_y \\ A_z \end{pmatrix}, \quad (\text{A.1})$$

$$\begin{pmatrix} B_{rr} & B_{r\phi} & B_{rz} \\ B_{\phi r} & B_{\phi\phi} & B_{\phi z} \\ B_{zr} & B_{z\phi} & B_{zz} \end{pmatrix} = \mathbf{U} \cdot \begin{pmatrix} B_{xx} & B_{xy} & B_{xz} \\ B_{yx} & B_{yy} & B_{yz} \\ B_{zx} & B_{zy} & B_{zz} \end{pmatrix} \cdot \mathbf{U}^\dagger, \quad (\text{A.2})$$

where

$$\mathbf{U} = \begin{pmatrix} x/r & y/r & 0 \\ -y/r & x/r & 0 \\ 0 & 0 & 1 \end{pmatrix} \quad (\text{A.3})$$

is a unitary matrix and \mathbf{U}^\dagger is its transpose.

In general, the divergence of a vector \mathbf{A} in cylindrical coordinates is [28]

$$\nabla \cdot \mathbf{A} = \frac{1}{r} \frac{\partial}{\partial r} (rA_r) + \frac{1}{r} \frac{\partial}{\partial \phi} A_\phi + \frac{\partial}{\partial z} A_z. \quad (\text{A.4})$$

The cylindrical components of the divergence of a tensor \mathbf{B} are [28]

$$(\nabla \cdot \mathbf{B})_r = \frac{1}{r} \frac{\partial}{\partial r} (rB_{rr}) + \frac{1}{r} \frac{\partial}{\partial \phi} B_{\phi r} + \frac{\partial}{\partial z} B_{zr} - \frac{1}{r} B_{\phi\phi}, \quad (\text{A.5})$$

$$(\nabla \cdot \mathbf{B})_\phi = \frac{1}{r} \frac{\partial}{\partial r} (rB_{r\phi}) + \frac{1}{r} \frac{\partial}{\partial \phi} B_{\phi\phi} + \frac{\partial}{\partial z} B_{z\phi} + \frac{1}{r} B_{\phi r}, \quad (\text{A.6})$$

$$(\nabla \cdot \mathbf{B})_z = \frac{1}{r} \frac{\partial}{\partial r} (rB_{rz}) + \frac{1}{r} \frac{\partial}{\partial \phi} B_{\phi z} + \frac{\partial}{\partial z} B_{zz}. \quad (\text{A.7})$$

In the Poiseuille problem the cylindrical components of the flow velocity \mathbf{u} , the heat flux \mathbf{q} and the pressure tensor \mathbf{P} depend on the radial variable r only. Consequently,

$$\nabla \cdot \mathbf{q} = \frac{1}{r} \frac{\partial}{\partial r} (r q_r), \quad (\text{A.8})$$

$$(\nabla \cdot \mathbf{P})_r = \frac{1}{r} \frac{\partial}{\partial r} (r P_{rr}) - \frac{1}{r} P_{\phi\phi}, \quad (\text{A.9})$$

$$(\nabla \cdot \mathbf{P})_\phi = 0, \quad (\text{A.10})$$

$$(\nabla \cdot \mathbf{P})_z = \frac{1}{r} \frac{\partial}{\partial r} (r P_{rz}), \quad (\text{A.11})$$

$$\mathbf{P} : \nabla \mathbf{u} = P_{rz} \frac{\partial u_z}{\partial r}. \quad (\text{A.12})$$

In Eq. (A.10) we have taken into account that, by symmetry, $P_{r\phi} = P_{\phi r} = 0$.

B Solution of the hierarchy of moment equations

In this Appendix we outline the steps needed to solve the hierarchy (49) with the profiles (51)–(54). To do so, we proceed sequentially from a given order s to the next order $s + 1$. It is also necessary to use the consistency relation

$$p = \frac{1}{3} (M_{2,0,0} + M_{0,2,0} + M_{0,0,2}) \quad (\text{B.1})$$

to any order in g . Let us start from the first-order equations.

B.1 First order in g ($s = 1$)

Setting $s = 1$, Eq. (49) becomes

$$\begin{aligned} \frac{\partial}{\partial x} M_{k_1+1, k_2, k_3}^{(1)} + \frac{\partial}{\partial y} M_{k_1, k_2+1, k_3}^{(1)} + k_3 \frac{\partial u^{(1)}}{\partial x} M_{k_1+1, k_2, k_3-1}^{(0)} \\ + k_3 \frac{\partial u^{(1)}}{\partial y} M_{k_1, k_2+1, k_3-1}^{(0)} - k_3 M_{k_1, k_2, k_3-1}^{(0)} = J_{\mathbf{k}}^{(1)}. \end{aligned} \quad (\text{B.2})$$

Next, inserting (53) and (54) into (B.2), we obtain

$$\begin{aligned} \chi_{k_1+1,k_2,k_3}^{(1,1,0)} + \chi_{k_1,k_2+1,k_3}^{(1,0,1)} + 2k_3 M_{k_1+1,k_2,k_3-1}^{(0)} u_2^{(1)} x + 2k_3 M_{k_1,k_2+1,k_3-1}^{(0)} u_2^{(1)} y \\ - k_3 M_{k_1,k_2,k_3-1}^{(0)} = J_{\mathbf{k}}^{(1,0,0)} + J_{\mathbf{k}}^{(1,1,0)} x + J_{\mathbf{k}}^{(1,0,1)} y, \end{aligned} \quad (\text{B.3})$$

where $J_{\mathbf{k}}^{(s,i,j)}$ is defined by Eq. (55). Equating the coefficients of the same degree in x and y , Eq. (B.3) decouples into the following set of equations:

$$2k_3 M_{k_1+1,k_2,k_3-1}^{(0)} u_2^{(1)} = J_{k_1,k_2,k_3}^{(1,1,0)}, \quad (\text{B.4})$$

$$2k_3 M_{k_1,k_2+1,k_3-1}^{(0)} u_2^{(1)} = J_{k_1,k_2,k_3}^{(1,0,1)}, \quad (\text{B.5})$$

$$\chi_{k_1+1,k_2,k_3}^{(1,1,0)} + \chi_{k_1,k_2+1,k_3}^{(1,0,1)} - k_3 M_{k_1,k_2,k_3-1}^{(0)} = J_{k_1,k_2,k_3}^{(1,0,0)}. \quad (\text{B.6})$$

Let us start with the moments of small degree ($k = 2$). For example, by taking $\{k_1, k_2, k_3\} = \{1, 0, 1\}$ in (B.4) and $\{k_1, k_2, k_3\} = \{0, 1, 1\}$ in (B.5,) we obtain

$$2u_2^{(1)} = -\chi_{1,0,1}^{(1,1,0)}, \quad (\text{B.7})$$

$$2u_2^{(1)} = -\chi_{0,1,1}^{(1,0,1)}. \quad (\text{B.8})$$

Now we insert the above equations into Eq. (B.6) with $\{k_1, k_2, k_3\} = \{0, 0, 1\}$. This allows us to obtain the coefficient of the flow velocity profile to first order in g :

$$u_2^{(1)} = -\frac{1}{4}. \quad (\text{B.9})$$

The process of solution continues in the same manner for the coefficients of moments of degree $k > 2$. We use the relations (B.4) and (B.5) in a first stage to determine the coefficients $\chi_{\mathbf{k}}^{(1,1,0)}$ and $\chi_{\mathbf{k}}^{(1,0,1)}$ with $k = 4$. In the second stage, the obtained results are inserted into (B.6) to evaluate the coefficients of degree $k = 3$. The same steps can continue infinitely by following the routes $k = 6 \rightarrow k = 5$; $k = 8 \rightarrow k = 7$; \dots . It is not necessary to evaluate all the coefficients, but some of them are essential to the solution of the problem to the next order in g .

B.2 Second order in g ($s = 2$)

As done in the first-order evaluation, let us take $s = 2$ in Eq. (49) and insert Eqs. (51)–(54). We then obtain an equation more complicated than that of the first order. Of course, the symmetry property $\chi_{\mathbf{k}}^{(s,i,j)} = 0$ if $i + k_1 = \text{odd}$ or $j + k_2 = \text{odd}$ must be applied. By equating the coefficients of the same degree in x and y we get the following set of algebraic equations:

a) $i + j = 4$

$$0 = J_{\mathbf{k}}^{(2,i,j)}, \quad (\text{B.10})$$

b) $i + j = 3$

$$(i + 1)\chi_{k_1+1,k_2,k_3}^{(2,i+1,j)} + (j + 1)\chi_{k_1,k_2+1,k_3}^{(2,i,j+1)} = J_{\mathbf{k}}^{(2,i,j)}, \quad (\text{B.11})$$

c) $i + j = 2$

$$(i + 1)\chi_{k_1+1,k_2,k_3}^{(2,i+1,j)} + (j + 1)\chi_{k_1,k_2+1,k_3}^{(2,i,j+1)} + 2k_3 u_2^{(1)} \left[\chi_{k_1+1,k_2,k_3-1}^{(1,i-1,j)} + \chi_{k_1,k_2+1,k_3-1}^{(1,i,j-1)} \right] = J_{\mathbf{k}}^{(2,i,j)}, \quad (\text{B.12})$$

d) $i + j = 1$

$$(i + 1)\chi_{k_1+1,k_2,k_3}^{(2,i+1,j)} + (j + 1)\chi_{k_1,k_2+1,k_3}^{(2,i,j+1)} + 2k_3 u_2^{(1)} \left[\chi_{k_1+1,k_2,k_3-1}^{(1,i-1,j)} + \chi_{k_1,k_2+1,k_3-1}^{(1,i,j-1)} \right] - k_3 \chi_{k_1,k_2,k_3-1}^{(1,i,j)} = J_{\mathbf{k}}^{(2,i,j)}, \quad (\text{B.13})$$

e) $i + j = 0$

$$\chi_{k_1+1,k_2,k_3}^{(2,1,0)} + \chi_{k_1,k_2+1,k_3}^{(2,0,1)} - k_3 \chi_{k_1,k_2,k_3-1}^{(1,0,0)} = J_{\mathbf{k}}^{(2,0,0)}. \quad (\text{B.14})$$

In the above equations the convention $\chi_{\mathbf{k}}^{(2,i,j)} = 0$ if $i < 0$ or $j < 0$ is implicitly understood.

According to the system (B.11)–(B.14), the coefficients of degree $k + 1$ with $i + j = \alpha + 1$ determine those of degree k with $i + j = \alpha$. For instance, Eq. (B.10) allows one to determine the coefficients with $k = 4$ and $i + j = 4$. The results obtained are inserted into (B.11) to determine the coefficients of degree $k = 3$ and $i + j = 3$. Then we go to Eq. (B.12) in order to determine those of degree $k = 2$ and $i + j = 2$. In general, the process of solution is done according to the following scheme:

$$\{\chi_k^{(2,i+j=4)}\} \rightarrow \{\chi_{k-1}^{(2,i+j=3)}\} \rightarrow \{\chi_{k-2}^{(2,i+j=2)}\} \rightarrow \{\chi_{k-3}^{(2,i+j=1)}\} \rightarrow \{\chi_{k-4}^{(2,i+j=0)}\}, \quad (\text{B.15})$$

where $\{\chi_k^{(2,\alpha)}\}$ denotes the set of coefficients of the same degree, namely $\{\chi_k^{(2,\alpha)}\} \equiv \{\chi_{\mathbf{k}}^{(2,i,j)}; k_1 + k_2 + k_3 = k, i + j = \alpha\}$. The expression of $J_{\mathbf{k}}^{(2,i,j)}$ is a linear combination of the coefficients $\chi_{\mathbf{k}}^{(2,i,j)}$, $T_4^{(2)}$, $T_2^{(2)}$ and $p_2^{(2)}$. Once a row k of the chain (B.15) is solved, it is necessary to go to the following row $k + 2$. This process continues until all the coefficients of the required profiles are completely determined. The results for the pressure and temperature are

$$p^{(2)} = \frac{3}{10}r^2, \quad T^{(2)} = \frac{34}{175}r^2 - \frac{1}{240}r^4. \quad (\text{B.16})$$

B.3 Third and fourth orders in g ($s = 3, 4$)

The process to third order in g is practically the same as the previous one. Since the pressure and the temperature are even functions of g , only the coefficients of u_z appear at this level. The result is

$$u^{(3)} = u_2^{(3)}r^2 - \frac{4\,429}{50\,400}r^4 - \frac{1}{2\,160}r^6, \quad (\text{B.17})$$

where the coefficient $u_2^{(3)} = -6.0806\dots$ is related to the ratio A_4/A_2 .

The calculation algorithm is essentially the same for the higher orders in g . However, the equations become more and more cumbersome and their solution requires a considerable computational effort. Here we give the final results for the pressure and the temperature to fourth order:

$$p^{(4)} = p_2^{(4)}r^2 + p_4^{(4)}r^4 + \frac{7}{7\,200}r^6, \quad (\text{B.18})$$

$$T^{(4)} = T_2^{(4)}r^2 + T_4^{(4)}r^4 - \frac{30\,931}{13\,608\,000}r^6 - \frac{23}{691\,200}r^8, \quad (\text{B.19})$$

where $p_2^{(4)} = -24.160\dots$, $p_4^{(4)} = -0.062666\dots$, $T_2^{(4)} = -59.511\dots$ and $T_4^{(4)} = -0.52856\dots$. The high values of $|p_2^{(4)}|$ and $|T_2^{(4)}|$ suggest that the series (44)–(47) are only asymptotic, in agreement with the situation in the case of the BGK model [8].

Along with the hydrodynamic fields, we have obtained all the moments of degrees $k = 3$ and $k = 4$ to third order in g . This allows us to get the pressure tensor and the heat flux. Their expressions in cylindrical coordinates are given in Sec. 5.

References

- [1] D. J. Tritton, *Physical Fluid Dynamics* (Oxford University Press, Oxford, 1988); G. K. Batchelor, *An Introduction to Fluid Dynamics* (Cambridge University Press, Cambridge, 1967); R. B. Bird, W. E. Stewart and E. W. Lightfoot, *Transport Phenomena* (Wiley, New York, 1960); H. Lamb, *Hydrodynamics* (Dover, New York, 1945).
- [2] L. P. Kadanoff, G. R. McNamara and G. Zanetti, “A Poiseuille viscometer for lattice gas automata,” *Complex Syst.* **1**, 791 (1987); “From automata to fluid flow: Comparison of simulation and theory,” *Phys. Rev. A* **40**, 4527 (1989).

- [3] R. Esposito, J. L. Lebowitz and R. Marra, “A hydrodynamic limit of the stationary Boltzmann equation in a slab,” *Commun. Math. Phys.* **160**, 49 (1994).
- [4] K. P. Travis, B. D. Todd and D. J. Evans, “Poiseuille flow of molecular fluids,” *Physica A* **240**, 315 (1997).
- [5] M. Alaoui and A. Santos, “Poiseuille flow driven by an external force,” *Phys. Fluids A* **4**, 1273 (1992).
- [6] M. Tij and A. Santos, “Perturbation analysis of a stationary nonequilibrium flow generated by an external force,” *J. Stat. Phys.* **76**, 1399 (1994). Note a misprint in Eq. (59): the denominators 25, 30, 3125, 750 and 250 should be multiplied by 3, 5, 3, 5 and 7, respectively.
- [7] M. Malek Mansour, F. Baras and A. L. Garcia, “On the validity of hydrodynamics in plane Poiseuille flows,” *Physica A* **240**, 255 (1997).
- [8] M. Tij, M. Sabbane and A. Santos, “Nonlinear Poiseuille flow in a gas,” *Phys. Fluids* **10**, 1021 (1998).
- [9] D. Risso and P. Cordero, “Generalized hydrodynamics for a Poiseuille flow: theory and simulations,” *Phys. Rev. E* **58**, 546 (1998).
- [10] S. Hess and M. Malek Mansour, “Temperature profile of a dilute gas undergoing a plane Poiseuille flow,” *Physica A* **272**, 481 (1999).
- [11] F. J. Uribe and A. L. Garcia, “Burnett description for plane Poiseuille flow,” *Phys. Rev. E* **60**, 4063 (1999).
- [12] K. Aoki, S. Takata and T. Nakanishi, “A Poiseuille-type flow of a rarefied gas between two parallel plates driven by a uniform external force,” *Phys. Rev. E* **65**, 026315 (2002).
- [13] P. Cordero and D. Risso, “Nonlinear effects in gases due to strong gradients,” in *Rarefied Gas Dynamics: 22nd International Symposium*, edited by T. J. Bartel and M. A. Gallis (American Institute of Physics, 2001).
- [14] B. D. Todd and D. J. Evans, “Temperature profile for Poiseuille flow,” *Phys. Rev. E* **55**, 2800 (1997); G. Ayton, O. G. Jepps and D. J. Evans, “On the validity of Fourier’s law in systems with spatially varying strain rates,” *Mol. Phys.* **96**, 915 (1999).
- [15] Y. Zheng, A. L. Garcia and B. J. Alder, “Comparison of kinetic theory and hydrodynamics for Poiseuille flow,” *J. Stat. Phys.* **109**, 495 (2002).
- [16] M. Tij and A. Santos, “Non-Newtonian Poiseuille flow of a gas in a pipe,” *Physica A* **289**, 336 (2001).
- [17] U. Frisch, B. Hasslacher and Y. Pomeau, “Lattice-Gas Automata for the Navier-Stokes Equation,” *Phys. Rev. Lett.* **56**, 1505 (1986).
- [18] C. Cercignani, *The Boltzmann Equation and Its Applications* (Springer-Verlag, New York, 1988).

- [19] V. Garzó and A. Santos, *Kinetic Theory of Gases in Shear Flows. Nonlinear Transport* (Kluwer, Dordrecht), in press.
- [20] S. Chapman and T. G. Cowling, *The Mathematical Theory of Nonuniform Gases* (Cambridge University Press, Cambridge, 1970).
- [21] C. Truesdell and R. G. Muncaster, *Fundamentals of Maxwell's Kinetic Theory of a Simple Monatomic Gas* (Academic Press, New York, 1980).
- [22] J. A. McLennan, *Introduction to Nonequilibrium Statistical Mechanics* (Prentice Hall, Englewood Cliffs, 1989).
- [23] Z. Alterman, K. Frankowski and C. L. Pekeris, "Eigenvalues and eigenfunctions of the linearized Boltzmann collision operator for a Maxwell gas and for a gas of rigid spheres," *Astrophys. J., Supplement Series* **7**, 291 (1962).
- [24] M. Sabbane and M. Tij, "Calculation algorithm for the collisional moments of the Boltzmann equation for Maxwell molecules," *Comp. Phys. Comm.* **149**, 19 (2002).
- [25] J. V. Iribarne and H.-R. Cho, *Atmospheric Physics* (Kluwer, Dordrecht, 1980); J. W. Chamberlain, *Theory of Planetary Atmospheres. An Introduction to Their Physics and Chemistry* (Academic Press, New York, 1978).
- [26] For a similar analysis of the Boltzmann equation but for the Fourier flow, see M. Tij, V. Garzó and A. Santos, "Nonlinear heat transport in a dilute gas in the presence of gravitation," *Phys. Rev. E* **56**, 6729 (1997); "Influence of gravity on the thermal conductivity," in *Rarefied Gas Dynamics*, edited by R. Brun, R. Campargue, R. Gatignol and J.-C. Lengrand (Cépaduès, Toulouse, 1999).
- [27] Consider for instance a highly rarefied gas of argon atoms ($m = 6.63 \times 10^{-26}$ kg) treated as hard spheres of diameter 3.5 \AA . At a number density $n_0 = 10^{-20} \text{ m}^{-3}$ the mean free path is $\ell_0 = 0.028 \text{ m}$. If the temperature is $T_0 = 300 \text{ K}$, then the value $g = 0.1v_0^2/\ell_0$ is equivalent to $g = 2.24 \times 10^5 \text{ m/s}^2$.
- [28] H. L. Anderson, editor, *A Physicist's Desk Reference* (American Institute of Physics, New York, 1989), Ch. 1.